

## Bevel Modification Effect on Rectangular Patch for UWB Using Theory Characteristics Mode

Liya Yusrina Sabila<sup>1</sup>, Denti Agustina Damayanti<sup>2</sup>

<sup>1</sup> Program Studi Teknik Elektro, Universitas Ahmad Dahlan, Indonesia

<sup>2</sup> Program Studi Teknik Elektro, Universitas Diponegoro, Indonesia

### ARTICLE INFORMATION

#### History:

Dikirimkan 10 November 2022

Direvisi 30 November 2022

Diterima 17 December 2022

#### Keywords:

Antenna;  
Monopole;  
UWB;  
TCM

#### Corresponding Author:

Liya Yusrina Sabila,  
Universitas Ahmad Dahlan,  
Jalan Ring Road Selatan,  
Bantul Yogyakarta, Indonesia.  
Email:  
[liya.sabila@te.uad.ac.id](mailto:liya.sabila@te.uad.ac.id)

### ABSTRACT / ABSTRAK

Ultra-wideband (UWB) is a communications technology that operates on frequencies between 3.1 and 10.6 GHz and has a wide bandwidth. This paper aims to look at the radiation characteristics of the structure using the Theory Characteristic Mode on a rectangular antenna with bevel modifications at the end of the patch. It can be seen from the active mode at the appropriate frequency to validate the antenna performance results. It was found that the proposed antenna has four operational modes in the antenna design before modification and seven active modes in the antenna design after modification. The antenna is made of FR-4 material with a thickness of 1.575 mm and a dielectric constant of 4.3. The bandwidth in the error measurement is around 7 GHz and a frequency range of 3.18 - 10.915 GHz with an S<sub>11</sub> value of less than -10 and a VSWR value of less than 2.

*Ultra-wideband (UWB) adalah teknologi komunikasi yang beroperasi pada frekuensi antara 3,1 dan 10,6 GHz dan memiliki bandwidth yang sangat lebar. Makalah ini bertujuan untuk melihat karakteristik struktur radiasi menggunakan Theory Characteristic Mode pada antena rectangular dengan modifikasi bevel diujung patch. Untuk validasi hasil performansi antena dapat dilihat dari mode aktif pada frekuensi yang sesuai. Ditemukan bahwa antena yang diusulkan memiliki 4 mode aktif pada desain antena sebelum modifikasi dan 7 mode aktif pada desain antena sesudah modifikasi. Antena terbuat dari bahan FR-4 dengan ketebalan 1,575 mm dan konstanta dielektrik 4,3. Bandwidth yang dicapai pada pengukuran adalah disekitar 7 GHz dan rentang frekuensi 3,18 - 10,915 GHz dengan nilai S<sub>11</sub> kurang dari -10 dan nilai VSWR kurang dari 2.*

This work is licensed under a [Creative Commons Attribution-Share Alike 4.0](https://creativecommons.org/licenses/by-sa/4.0/)



#### Document Citation:

L. Y. Sabila and D. A. Damayanti, "Bevel Modification Effect on Rectangular Patch for UWB Using Theory Characteristics Mode," *Buletin Ilmiah Sarjana Teknik Elektro*, vol. 4, no. 2, pp. 86-93, 2022, DOI: [10.12928/biste.v4i2.6970](https://doi.org/10.12928/biste.v4i2.6970).

## 1. INTRODUCTION

The creation of ultrawideband radio technology (UWB) has applications in cognitive radio, radar, biological imaging, indoor localization, tracking, and high-level wireless data transmission systems [1]–[4]. Although antenna design considerations are usually determined by specific application and system considerations, in general, printed monopole antennas are small in size with return loss, gain, and radiation patterns that can produce extensive bandwidth. It is well known that UWB-printed monopole antennas offer exciting features such as a simple shape, an extensive bandwidth of more than 3 to 10 GHz, a small size, and ease of manufacturing [5]–[8].

Few antenna types addressed physical behavior employing Theory Characteristic Mode, even though several monopole antennas were manufactured with the best performance in previously published designs (TCM). TCM was first put forth by Garbacz [9]–[11] and later refined by Harrington [12], [13] roved by Harrington [12]–[13], who examined the behavior of antennas in their current mode to offer more physical explanations of the radiation phenomena that occur in structures. Several wire and planar antennas have been designed and successfully analyzed using TCM [14], [15]. In order to enhance performance at ultrawideband frequencies, TCM was employed in this design to provide physical insight into the transmitter behavior of the ultrawideband printed monopole antenna.

This design uses a printed monopole with a bevel-shaped modification. This effort was made to achieve UWB operation at a frequency of 3.1-10.6 GHz. The bevel angle varies at a specific angle, and performance is analyzed using TCM. Hasil end of antenna size with bevel-shaped modification,  $40 \times 45 \times 1.6 \text{ mm}^3$ , using FR-4 material with a thickness of 1.6 mm, and a dielectric constant of 4.3. The parameters studied on antenna design using TCM in CST Studio Suite 2019 software are  $S_{11}$  and VSWR.

## 2. METHODS

### 2.1. Antenna Monopole

A monopole antenna is a type of antenna made of a conductor attached to a dielectric. At the bottom, there is a ground plane, and at the top, there is a patch which is the part of the antenna that emits radiation. Figure 1 depicts the main components of a monopole antenna, which are a radiating element (radiator), a conducting patch, a dielectric substrate, and a ground plane. Similar requirements can be found in numerous other governmental and commercial uses, including wireless communications and mobile radio. The usage of monopole antennas can satisfy these requirements. Monopole antennas, as depicted in Figure 1, are made up of a thin metallic strip (patch) that is elevated slightly above the ground [16], [17]. Patch antennas are another name for monopole antennas that are frequently used. The feed lines and radiating elements are typically photo-etched onto the dielectric substrate. The radiating patch can be square, rectangular, thin strip (dipole), circular, elliptical, triangular, etc. The feed line feeding technique is also depicted in Figure 1. The monopole-line feed is simple to model, easy to construct, and easy to match by adjusting the inset location.

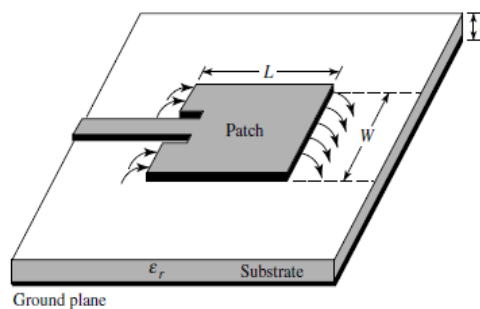


Figure 1. Monopole antenna structure

### 2.2. Theory Characteristic Mode (TCM)

Garbacz first established Theory Characteristic Mode (TCM), also known as Characteristic Mode Analysis (CMA), in 1968. Harrington and Mautz later obtained TCM. Perfect Electrical Conductor (PEC) is a material that is frequently utilized in this TCM [18]–[20]. PEC is the antenna body's conducting component. A current ( $J$ ) on the surface may result from the existence of an electric field ( $E$ ) striking the conductor body on the surface ( $S$ ). The CMA formula can be applied as a current relationship ( $J$ ) on the surface ( $S$ ) of the conducting material since this current surface will generate a scattered field. The impedance matrix and the generalized eigenvalue problem are used to determine the characteristic modes:

$$Z(J) = R(J) + jX(J) \quad (1)$$

$$X(\vec{J}_n) = \lambda_n R(\vec{J}_n) \quad (2)$$

Where  $\lambda_n$  is an eigenvalue,  $\vec{J}_n$  is eigencurrent, and  $R$  and  $X$  are real and imaginary parts of the impedance  $Z$ . The magnitude of the eigenvalues gives information about the resonant frequency and transmitter characteristics of various current modes, making them crucial. Modal significance and characteristic angle are two additional elements.

### 2.2.1. Modal Significance

Modal significance ( $MS_n$ ) represents the normalized amplitude in the current mode, which can be expressed as:

$$MS_n = \left| \frac{1}{1 + j\lambda} \right| \quad (3)$$

Equation (3) reflects the average amplitude of the active mode and is frequently referred to as the capital significance ( $MS_n$ ). This typical amplitude does not consider excitation and is solely dependent on the size and form of the conducting item.

### 2.2.2 Characteristic Angle

The characteristic angle is defined as:

$$\alpha_n = 180^\circ - \tan^{-1}(\lambda_n) \quad (4)$$

The mode is resonant when  $\lambda_n = 0$ , i.e., when the characteristic angle  $\lambda_n$  is  $180^\circ$ . Therefore, when the characteristic angle is close to  $180^\circ$ , the mode is a good radiator, while when the characteristic angle is close to  $90^\circ$  or  $270^\circ$ , this mode is mainly energy saving.

## 2.3. Specifications

Antenna specifications are an essential part of the design process. Determination of specifications adapted to the system and technology used. Following are the antenna design specifications.

1. The resonant frequency is at 3.1 GHz – 10.6 GHz.
2. Parameter  $S_{11} \leq -10$  dB at a frequency of 3.1GHz – 10.6 GHz.
3.  $VSWR \leq 2$  at a frequency of 3.1GHz – 10.6 GHz.

The specifications for the substrate and conductor materials used in the design of microstrip antennas are as follows:

- Dielectric material: Epoxy – FR 4
- Dielectric constant ( $\epsilon_r$ ): 4.4
- Dielectric thickness (h): 0.0016 m = 1.6 mm
- Substrate coating material (conductor): Copper
- Thickness of the conductor material (t): 0.035 mm
- Line characteristic impedance: 50  $\Omega$

## 3. RESULT AND DISCUSSION

### 3.1. Theory Characteristic Mode (TCM) of Initial Design

Figure 2 shows the initial design print monopole antenna before optimization (patch A), and Figure 3 shows the final design after optimization (patch B). The design sizes of patches A and B are shown in Table 1, and the patch material used on the TCM is PEC.

**Table 1.** Size of antenna design

Antenna	Size of parameter				
	A (mm)	B (mm)	C (mm)	D (mm)	$\alpha$ ( $^\circ$ )
Patch A	40	45	13.4	9.8	-
Patch B	40	45	17	20	5 $^\circ$

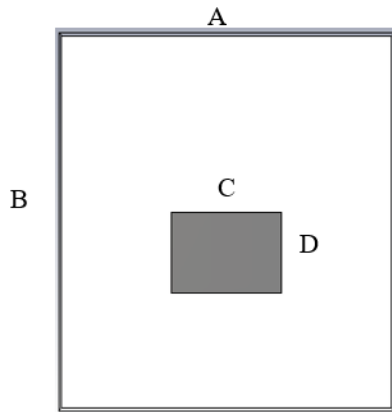


Figure 2. Patch A design

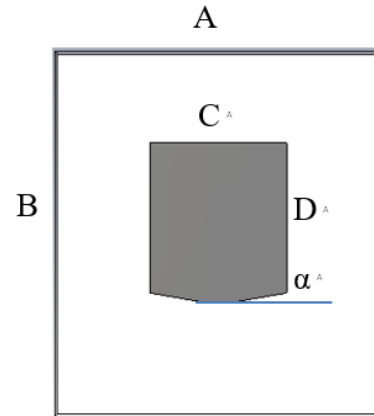


Figure 3. Desain Patch B design

3.1.1 Modal Significance

Figure 4 and Figure 5 show variations with the modal significance of the initial design and final design associated with active mode from the monopole antenna print patches A and B.

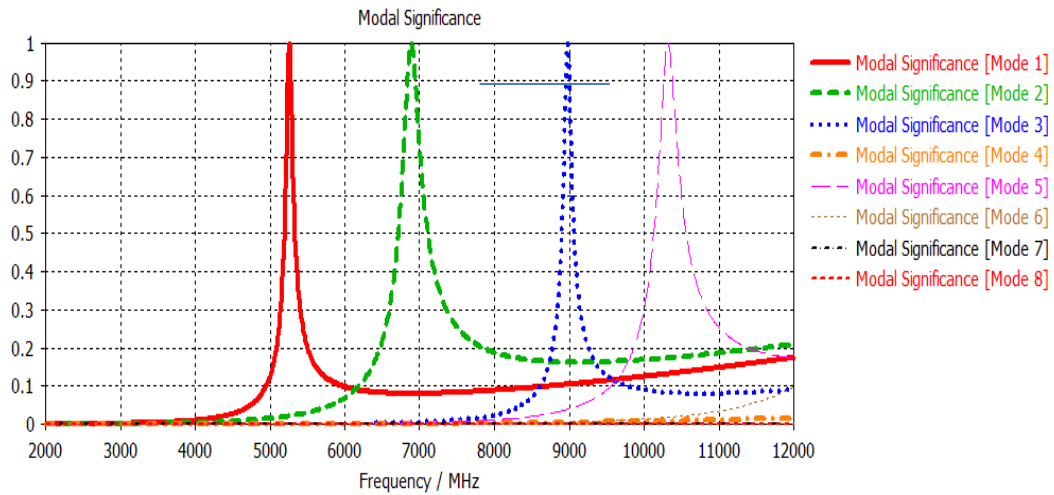


Figure 4. Modal significance of patch A (initial design)

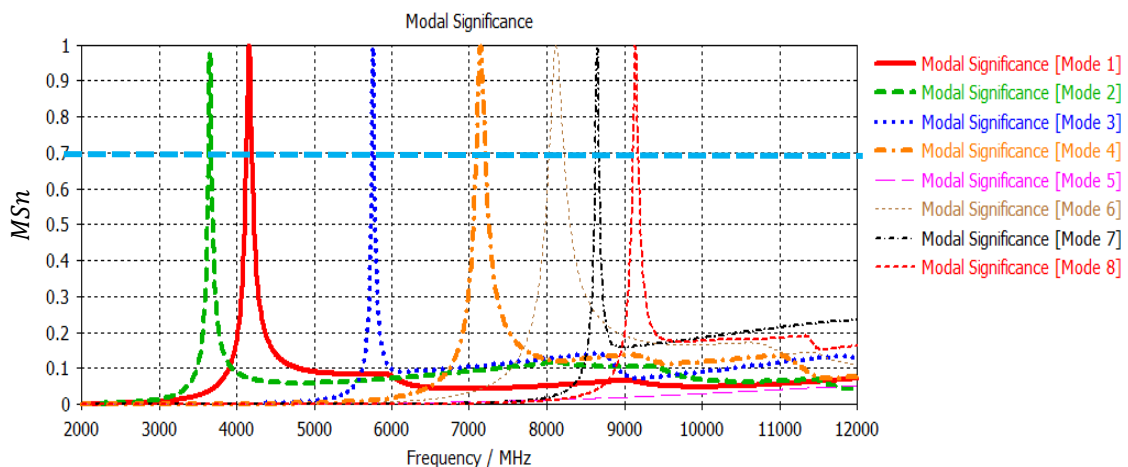


Figure 5. Modal significance of patch B (final design)

A maximum value of one in the capital significance curve indicates the resonance of each mode. This indicates that the most efficient mode for radiation is the curve that approaches the value of one. The breadth

of the capital significance curve close to the maximum point can then be used to determine the mode transmitter's bandwidth. The curve's maximum point limit is 0.707. The performance of the radiating mode can be assessed in part by its radiating bandwidth. The fraction of the frequency difference (minus top down) at the mode resonant frequency depicted in Table 2 can indicate the bandwidth radiation from the mode  $BW_n$ .

**Table 2.** Comparison of Modal significance of patch A and patch B

Mode	$F_{res}$ (MHz)		$F_u$ (MHz)		$F_L$ (MHz)		$BW_n$ (MHz)	
	Patch A	Patch B	Patch A	Patch B	Patch A	Patch B	Patch A	Patch B
1	5260	4160	5303	4190	5219	4130	0.016	0.014
2	6890	3650	7011	3670	6781	3640	0.033	0.008
3	8980	5760	9027	5770	8930	5740	0,011	0.005
4	-	7140	-	7200	-	7090	-	0,015
5	10320	-	10454	-	10202	-	0.024	-
6	-	8120	-	8210	-	8040	-	0.021
7	-	8650	-	8670	-	8630	-	0.005
8	-	9140	-	9170	-	9110	-	0.007

**3.1.2 Characteristic Angle**

The characteristic angle represents the phase angle between the characteristic current  $J_n$  and the distinct regions  $En$ . Figure 6 and Figure 7 present variations with characteristic angles ( $\alpha_n$ ) associated with the current printed monopole antenna mode. It is known that the mode reverberates when  $\lambda_n = 0$ , i.e., when the characteristic angle  $\alpha_n$  is  $180^\circ$ . Table 3 is the result of calculating the bandwidth emitted by the mode with characteristic angles,  $fH$  and  $fL$  is the frequency whose characteristic angles are at  $135^\circ$  and  $225^\circ$ . Only four modes out of seven are active in patch A, while in patch B, all modes are active. The more modes, the wider the resulting bandwidth.

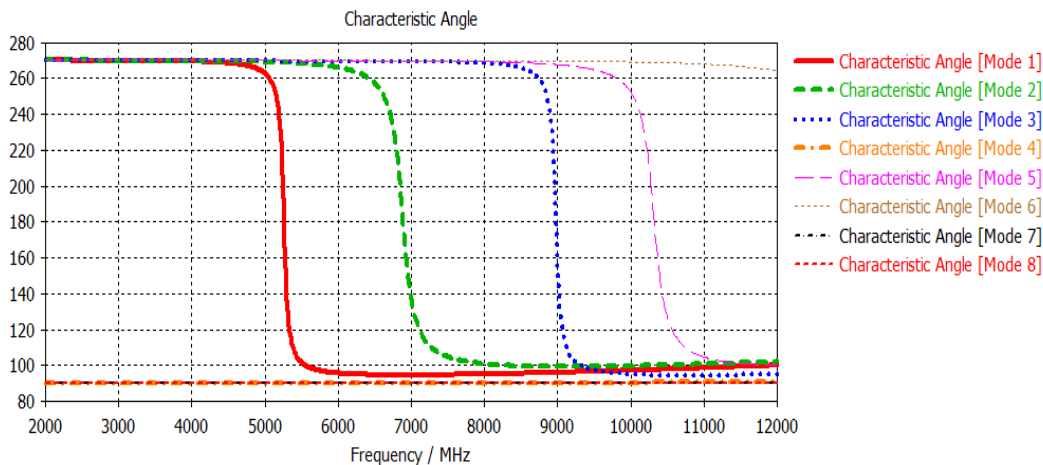


**Figure 6.** Characteristic Angel of patch A (initial design).

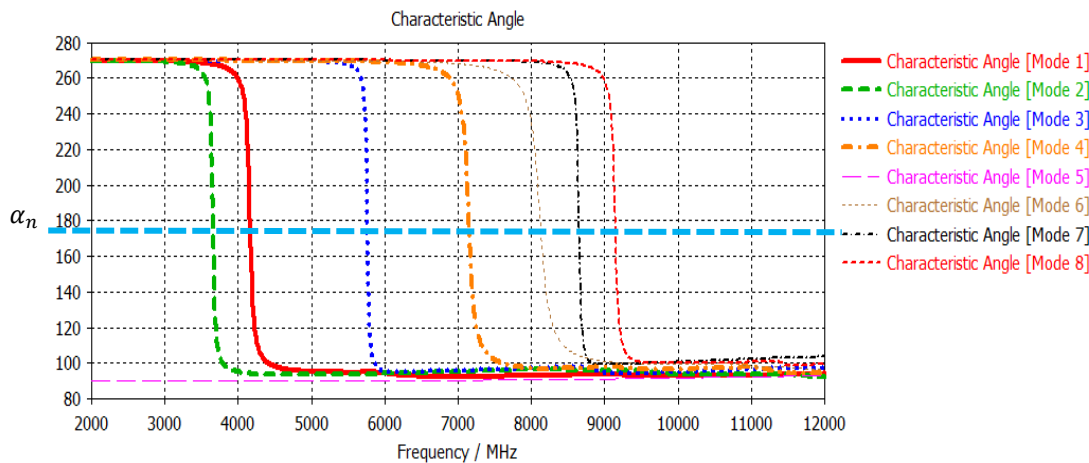


**Figure 7.** Characteristic Angel of patch B (final design).

**Table 3.** Comparison of Characteristics angle patch A and patch B

Mode	$F_{res}$ (MHz)		$F_H$ (MHz)		$F_L$ (MHz)		$BW_n$ (MHz)	
	Patch A	Patch B	Patch A	Patch B	Patch A	Patch B	Patch A	Patch B
1	5260	4160	5302	4200	5220	4130	0.016	0.017
2	6887	3650	7008	3680	6782	3630	0.033	0.014
3	8976	5760	9026	5780	8930	5740	0.011	0.007
4	-	7140	-	7200	-	6090	-	0.156
5	10319	-	10451	-	10204	-	0.024	-
6	-	8120	-	8220	-	8030	-	0.023
7	-	8650	-	8670	-	8620	-	0.006
8	-	9140	-	9180	-	9110	-	0.008

**3.2. Printed Monopole Antenna Measurement**

**3.2.1.  $S_{11}$**

$S_{11}$  on the antenna is measured using the Advantest R3770 Network Analyzer.  $S_{11}$  and VSWR analysis is possible with Vector Network Analyzer devices. The results of the measurements are presented as a frequency graph against time for further analysis. A curve graph displaying the measurement results  $S_{11}$  and VSWR is shown. An image was created in a graph showing the relationship between frequency and magnitude in decibel units using the measurement of  $S_{11}$  (dB). The frequency range is displayed on the horizontal axis as 2.5–11 GHz, with a box width (span) of 850 MHz. As illustrated in Figure 8, the vertical axis of  $S_{11}$  has a width of one box of 10dB. The differences between the findings of the  $S_{11}$  measurements and the Simulated  $S_{11}$  results are thus visible, as shown in Table 4.

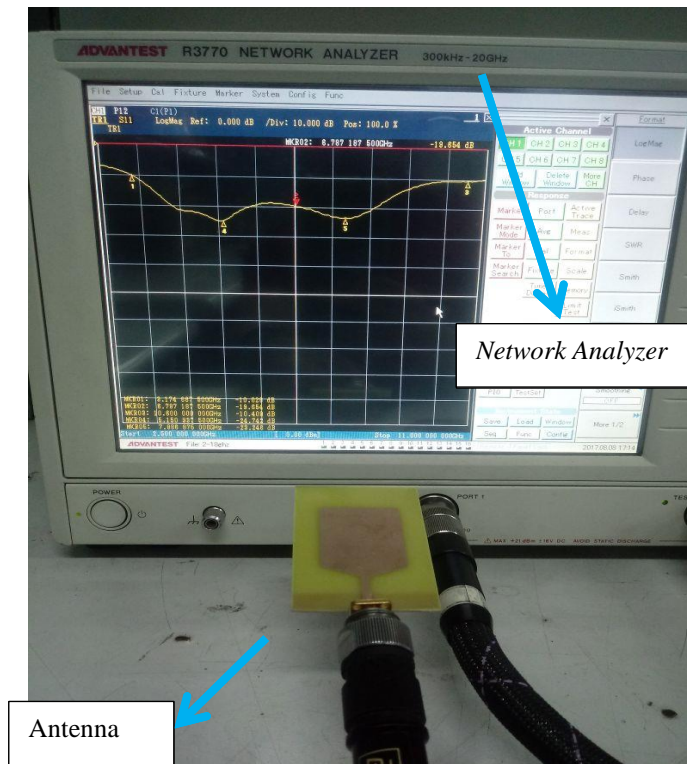


**Figure 8.** Configure measurement with *Network Analyzer*

**Table 4.** Frequency on  $S_{11} = -10$  dB printed monopole antenna.

Frequency	$S_{11} = -10$ dB	
	Simulation	Measurement
Lower Frequency	2.5	3.1
Upper Frequency	10.6	10.9

Table 4 shows the frequency when  $S_{11}$  is equal to -10 in the simulation and measurements of printed monopole antennas. The lower frequency in the simulation is at 2.5 GHz, while the measurement is at 3.1 GHz. There is a shift in the measurement's lower frequency by 0.6 GHz, but it still meets the specifications. The

measurements of  $S_{11}$  for each resonant frequency of the printed monopole antenna are shown in Table 5. The resonant frequency is determined based on the lower frequency, upper frequency, and on the  $S_{11}$  of the measurement. Although there is a shift, the *bandwidth* results on measurements of 3.1-10.9 GHz have met the specified specifications.

**Table 5.** Comparison of  $S_{11}$  of simulation and measurement

Resonance Frequency	Frequency (GHz)	$S_{11}$ (dB)	
		Simulation	Measurement
$Fr_1$	3.1	-12.2	-10.1
$Fr_2$	4.0	-27.5	-20.0
$Fr_3$	5.0	-10.8	-24.6
$Fr_4$	7.7	-18.8	-23.1
$Fr_5$	10.9	-8.9	-10.1

### 3.2.2. VSWR

The results of the simulation and measurement of VSWR are shown in Table 6. A comparison of the simulation and measurements shows that  $VSWR \leq 2$  in measurements achieved are at a frequency of 3.17-10.9 GHz while in the simulation of 2.5-10.6 GHz. Differences in VSWR between the simulation and measurements and shifts in resonant frequency are caused by the permittivity of the dielectric material of FR-4. The dielectric material of FR-4 fabrication is smaller than FR-4 in simulation, so the frequency shifts upwards.

**Table 6.** Comparison of VSWR of simulation and measurement

Resonance Frequency	Frequency (GHz)	VSWR < 2	
		Simulation	Measurement
$Fr_1$	3.1	1.6	1.9
$Fr_2$	4.0	1.1	1.2
$Fr_3$	5.0	1.8	1.1
$Fr_4$	7.7	1.3	1.1
$Fr_5$	10.9	2.1	1.9

## 4. CONCLUSIONS

In the analysis using theory characteristic mode, after modification width, length, and bevel to the patch, the results of significant modal and characteristic angles have reached maximum values at low frequencies of 3.0-4.0 GHz and high frequencies of 6, 0-10.0 GHz so it can resonate and dominate the radiation which affects ultrawideband frequencies of 3.1-10.6 GHz. The printed monopole antenna measurement bandwidth is 7.8 GHz, and the monopole antenna simulation is 8.3 GHz. The simulation results have a wider bandwidth than the measurement.

## REFERENCES

- [1] O. P. Kumar, P. Kumar, T. Ali, P. Kumar, and S. Vincent, "Ultrawideband Antennas: Growth and Evolution," *Micromachines*, vol. 13, no. 1, 2022, <https://doi.org/10.3390/mi13010060>.
- [2] D. Minoli and B. Occhiogrosso, "Ultrawideband (UWB) Technology for Smart Cities IoT Applications," *2018 IEEE Int. Smart Cities Conf. ISC2 2018*, pp. 1–8, 2019, <https://doi.org/10.1109/ISC2.2018.8656958>.
- [3] N. Anveshkumar, A. S. Gandhi, and V. Dhasarathan, "Cognitive radio paradigm and recent trends of antenna systems in the UWB 3.1–10.6 GHz," *Wirel. Networks*, vol. 26, no. 5, pp. 3257–3274, 2020, <https://doi.org/10.1007/s11276-019-02245-7>.
- [4] A. Basir and H. Yoo, "A Stable Impedance-Matched Ultrawideband Antenna System Mitigating Detuning Effects for Multiple Biotelemetric Applications," *IEEE Trans. Antennas Propag.*, vol. 67, no. 5, pp. 3416–3421, 2019, <https://doi.org/10.1109/TAP.2019.2905891>.
- [5] O. Manoochehri, A. Darvazehban, M. A. Salari, A. Emadeddin and D. Erricolo, "A Parallel Plate Ultrawideband Multibeam Microwave Lens Antenna," *IEEE Transactions on Antennas and Propagation*, vol. 66, no. 9, pp. 4878–4883, Sept. 2018, <https://doi.org/10.1109/TAP.2018.2845548>.
- [6] A. B. Dey, S. S. Pattanayak, D. Mitra, and W. Arif, "Investigation and design of enhanced decoupled UWB MIMO antenna for wearable applications," *Microw. Opt. Technol. Lett.*, vol. 63, no. 3, pp. 845–861, 2021, <https://doi.org/10.1002/mop.32699>.
- [7] S. C. Puri, S. Das, and M. G. Tiary, "UWB monopole antenna with dual-band-notched characteristics," *Microw. Opt. Technol. Lett.*, vol. 62, no. 3, pp. 1222–1229, 2020, <https://doi.org/10.1002/mop.32112>.
- [8] M. N. Hasan, S. Chu, and S. Bashir, "A DGS monopole antenna loaded with U-shape stub for UWB MIMO applications," *Microw. Opt. Technol. Lett.*, vol. 61, no. 9, pp. 2141–2149, 2019, <https://doi.org/10.1002/mop.31877>.
- [9] J. B. Kamili and A. Bhattacharya, "Design of a Novel Compact Bowtie Antenna and Analysis Using Characteristic Modes," *IEEE Reg. 10 Annu. Int. Conf. Proceedings/TENCON*, vol. 2019-October, pp. 1903–1907, 2019, <https://doi.org/10.1109/TENCON.2019.8929474>.

- [10] H. Wallén, P. Ylä-Oijala, D. C. Tzarouchis, and A. Sihvola, "Mie Scattering and Characteristic Modes of Lossy Dielectric Objects," *2018 2nd URSI Atl. Radio Sci. Meet. AT-RASC 2018*, no. June, pp. 2–5, 2018, <https://doi.org/10.23919/URSI-AT-RASC.2018.8471401>.
- [11] A. Ghalib and M. S. Sharawi, "New antenna mode generation based on theory of characteristic modes," *Int. J. RF Microw. Comput. Eng.*, vol. 29, no. 6, pp. 1–8, 2019, <https://doi.org/10.1002/mmce.21686>.
- [12] M. Khan, "Feed based bandwidth enhancement of u-slot microstrip patch using theory of characteristic modes," *2019 IEEE Int. Symp. Antennas Propag. Usn. Radio Sci. Meet. APSURSI 2019 - Proc.*, pp. 257–258, 2019, <https://doi.org/10.1109/APUSNCURSINRSM.2019.8889327>.
- [13] S. Huang, J. Pan, and D. Yang, "A Novel Electromagnetic Power-Based Characteristic Mode for Magnetodielectric Materials," *Radio Sci.*, vol. 53, no. 4, pp. 458–471, 2018, <https://doi.org/10.1002/2018RS006532>.
- [14] A. Ghalib, R. Hussain, and M. S. Sharawi, "Analysis of slot-based radiators using TCM and its application in MIMO antennas," *Int. J. RF Microw. Comput. Eng.*, vol. 29, no. 2, pp. 1–17, 2019, <https://doi.org/10.1002/mmce.21544>.
- [15] F. H. Lin and Z. N. Chen, "A Method of Suppressing Higher Order Modes for Improving Radiation Performance of Metasurface Multiport Antennas Using Characteristic Mode Analysis," *IEEE Trans. Antennas Propag.*, vol. 66, no. 4, pp. 1894–1902, 2018, <https://doi.org/10.1109/TAP.2018.2806401>.
- [16] T. K. Saha, C. Goodbody, T. Karacolak, and P. K. Sekhar, "A compact monopole antenna for ultra-wideband applications," *Microw. Opt. Technol. Lett.*, vol. 61, no. 1, pp. 182–186, 2019, <https://doi.org/10.1002/mop.31519>.
- [17] S. U. Rahman, Q. Cao, H. Ullah, and H. Khalil, "Compact design of trapezoid shape monopole antenna for SWB application," *Microw. Opt. Technol. Lett.*, vol. 61, no. 8, pp. 1931–1937, 2019, <https://doi.org/10.1002/mop.31805>.
- [18] P. Ylä-Oijala, "Generalized Theory of Characteristic Modes," *IEEE Trans. Antennas Propag.*, vol. 67, no. 6, pp. 3915–3923, 2019, <https://doi.org/10.1109/TAP.2019.2905794>.
- [19] B. Xiao, H. Wong, D. Wu, and K. L. Yeung, "Design of Small Multiband Full-Screen Smartwatch Antenna for IoT Applications," *IEEE Internet Things J.*, vol. 8, no. 24, pp. 17724–17733, 2021, <https://doi.org/10.1109/JIOT.2021.3082535>.
- [20] P. Ylä-Oijala, A. Lehtovuori, H. Wallén, and V. Viikari, "Coupling of Characteristic Modes on PEC and Lossy Dielectric Structures," *IEEE Trans. Antennas Propag.*, vol. 67, no. 4, pp. 2565–2573, 2019, <https://doi.org/10.1109/TAP.2019.2893300>.

#### AUTHOR BIOGRAPHY



**Liya Yusrina Sabila** received a B.Eng. degree in 2017 and a Master's degree in engineering in 2021 from Electrical Engineering Department at Diponegoro University, Semarang, Indonesia. Currently, I am working as a Junior Lecturer and a researcher at the Electrical Engineering Department, Faculty of Industrial Technology, Ahmad Dahlan University in Yogyakarta, Indonesia. My research interests are in antenna and propagation, especially small antenna design.



**Denti Agustina Damayanti** received a B.Eng. degree in 2017 from Electrical Engineering Department, Diponegoro University, Semarang, Indonesia. My research interests are in antenna and propagation, especially small antenna design.